NMR realization of adiabatic quantum algorithms for the modified Simon problem

Yu Long,[1] Guanru Feng,[1] Yongchao Tang,[1] Wei Qin,[1] and Guilu Long[1,2,*]

[1]*State Key Laboratory of Low-dimensional Quantum Physics and Department of Physics, Tsinghua University, 100084 Beijing, China*

[2]*Tsinghua National Laboratory for Information Science and Technology, Tsinghua University, 100084 Beijing, China*

(Received 27 March 2012; revised manuscript received 2 May 2013; published 9 July 2013)

Having the advantages of inherent robustness and fault tolerance, adiabatic quantum algorithms have attracted much attention in recent years. In this paper, we report the NMR experimental realization of adiabatic algorithms for the modified Simon's problem in a NMR quantum information processor. We first realized an adiabatic quantum algorithm by Rao [Phys. Rev. A **67**, 052306 (2003)] and then proposed a quantum algorithm by using the method of enhanced symmetry of the Hamiltonian given in Schaller and Schtzhold [Quantum Inf. Comput. **10**, 109 (2010)]. We demonstrated this symmetry-enhanced algorithm in experiment. We studied the effects of the number of Trotter evolution steps on the validity of adiabatic evolution and decoherence. In practical applications, a trade-off between pulse imperfection and adiabatic requirement must be made in the Trotter evolution step number. An optimal evolution step number and run time were indicated by our results. The experimental demonstration also showed that the symmetry-enhanced algorithm gave a better performance.

DOI: 10.1103/PhysRevA.88.012306 PACS number(s): 03.67.Lx, 33.25.+k

I. INTRODUCTION

It is expected that quantum computing will have great advantages over classical computing in problems, such as the prime factorization of large numbers and the unordered data searching problem [1,2]. Several models of quantum computing are currently being used, namely, the circuit model, the measurement-based model, the adiabatic evolution model, and others [3–7]. Instead of using a sequence of logic gates on the computational state as in the circuit model, an adiabatic quantum algorithm solves a computational problem through an adiabatic evolution of the ground state of a varying Hamiltonian. Adiabatic quantum computing provides an alternative approach to quantum algorithm design and has several advantages, including inherent robustness against control errors and decoherence [8]. Research on its algorithm design [6,9–14], time complexity [15,16], computational power [17–19], as well as its intrinsic fault tolerance and related stabilizer codes [8,20,21] has attracted much attention. It also stimulated studies on the quantum adiabatic theorem [22–30]. There have been increased efforts in the experimental realization of adiabatic algorithms, and the adiabatic versions of the Deutsch-Jozsa, Grover, and Shor algorithms have been experimentally demonstrated [31–36].

Adiabatic quantum computing exploits the evolution of a quantum state via a time-dependent Hamiltonian in which the initial state is the ground state of the initial Hamiltonian, and the ground state of the final Hamiltonian encodes the solution to the problem. Although it was shown that the quantum adiabatic condition was problematic in certain applications [22] and it is only a necessary but not a sufficient condition [23], it is still a good approximation, and its application on adiabatic quantum computation remains useful, except in some instances. The standard quantum adiabatic condition can be expressed as $T \gg \varepsilon/g_{\min}^2$, where T is the total evolution time, $g_{\min}$ is the minimal energy gap of the lowest two levels, and $\varepsilon = \max_{0\leqslant s\leqslant 1}|\langle l=1;s|dH/ds|l=0;s\rangle|$ is the transition amplitude between the ground state and the first excited state [33]. ε is on the order of a typical eigenvalue of the Hamiltonian with a moderate value [5]; thus, the size of T depends mainly on $g_{\min}^2$. The efficiency of the adiabatic quantum algorithm depends on the total evolution time, and the adiabatic model has been proven to be as powerful as the circuit model for quantum computations [17–19].

The modified Simon's problem (MSP) is a restricted version of Simon's problem [12,37], which is a discrete paradigm of the hidden subgroup problem (HSP) and is of great importance in mathematics and quantum computing. HSP plays a pivotal role in quantum computation, especially in Shor's quantum algorithm for factoring, the discrete logarithm, as well as in the quantum algorithms for the graph isomorphism problem and certain shortest vector problems [38,39]. An adiabatic quantum algorithm for MSP was proposed by Rao in 2003 [12,13]. Rao's algorithm belongs to a large kind of adiabatic algorithm, which has exponential complexity [40–42], and the time required to run the algorithm is exponential with the size of the problem.

In this paper, two adiabatic algorithms for the MSP, Rao's algorithm [12] and a symmetry-enhanced algorithm (SEA), proposed in this paper by using the enhanced Hamiltonian symmetry method given in Ref. [43], were demonstrated in a NMR quantum information processor.

We also studied the effect of decoherence and imperfections of gate operations. Considering an experimental control error, the actual Hamiltonian can be written as

$$\widetilde{H}(t) = H(t) + K(t), \tag{1}$$

where $H(t)$ is the approximate Hamiltonian used for the adiabatic algorithm simulated via unitary controls in the NMR system and $K(t)$ denotes the error that resulted from imperfect implementation [8]. In practice, the system also interacts with the environment and suffers decohering effects. With realizable experimental control and real decoherence, there is a trade-off in the number of steps of the evolution simulation. Increasing the number of Trotter steps may improve the accuracy of the simulation of the adiabatic evolution because the

*gllong@tsinghua.edu.cn

adiabatic condition is better satisfied, but meanwhile, this also requires more radio frequency pulses, and the imperfections of the pulses accumulate, causing greater errors. Therefore, a trade-off is required between satisfying the adiabatic condition and reducing the number of pulses. There should be an optimal step number, beyond which the breakdown of the adiabatic algorithm may occur [31]. In this paper, the experimental study of the optimal number of iterations is also performed.

The paper is organized as follows. After the introduction, MSP and the corresponding Rao's adiabatic quantum algorithm are discussed in Sec. II and are followed by a two-qubit example of the algorithm. We then give the SEA. In Sec. III, we present the experimental procedures of the two algorithms. In Sec. IV, we give the NMR experimental implementation of the two adiabatic algorithms. The experimental results are discussed, and the relation between the number of Trotter steps and the fidelity of the experimental result is investigated. In Sec. V, we give a conclusion.

II. ADIABATIC ALGORITHM FOR MSP

The MSP is defined as follows [12]: Given a function ϕ: $\{0,1\}^n \to \{0,1\}^{n-1}$ such that $\phi(x) = \phi(x')$ if and only if $x' = x \oplus h$, where $\oplus$ is a bitwise exclusive OR for $h \in \{0^n, c\}$, where $c \in \{0,1\}^n \setminus 0^n$. The problem is to find c.

A. Rao's adiabatic algorithm for MSP

Now, we briefly describe Rao's adiabatic algorithm for MSP. In Rao's algorithm, the initial Hamiltonian is

$$H_b = I - |\psi_b\rangle\langle\psi_b|, \tag{2}$$

where $|\psi_b\rangle$ is the ground state of H_b,

$$|\psi_b\rangle = \frac{1}{\sqrt{2^n - 1}} \sum_{z\in\{0,1\}^n\setminus 0^n} |z\rangle,$$

which is easy to construct. The final Hamiltonian is

$$H_f = \sum_{z\in\{0,1\}^n} \left(\frac{|\phi(x) - \phi(x \oplus z)|}{N} + (1 - \delta_{\phi(x),\phi(x\oplus z)})n \right) \times |z\rangle\langle z|, \tag{3}$$

where $\phi(x)$ is calculated from the black box and the ground state of H_f encodes the solution to the MSP. With the initial and final Hamiltonians, the total time-dependent Hamiltonian is defined as

$$H(s) = (1 - s)H_b + sH_f, \tag{4}$$

which is the linear interpolation of the initial and final Hamiltonians, where $s = t/T$ and $0 \leqslant s \leqslant 1$ with T representing the total evolution time. Starting from the initial state, which is the ground state of H_b, the evolved quantum state remains in the ground state of the slowly varying Hamiltonian $H(s)$, until the final state at $s = 1$, which encodes the solution to the problem.

For a two-bit case of the MSP, the function $\phi(x)$ in this case is given in Table I.

TABLE I. MSP for two qubits.

x	00	01	10	11
$\phi(x)$	0	1	0	1

In Rao's adiabatic algorithm, the initial Hamiltonian in this case is

$$H'_{b1} = I - |\psi_{b1}\rangle\langle\psi_{b1}| = I - 1/3 \begin{pmatrix} 0 & 0 & 0 & 0 \\ 0 & 1 & 1 & 1 \\ 0 & 1 & 1 & 1 \\ 0 & 1 & 1 & 1 \end{pmatrix}. \tag{5}$$

The ground state of H'_{b1} is $|\psi_{b1}\rangle = (0,1,1,1)^T$, which is a linear superposition of the two-qubit computational basis states, except for $|00\rangle$. The final Hamiltonian is

$$H_{f1} = 9/4 \begin{pmatrix} 0 & 0 & 0 & 0 \\ 0 & 1 & 0 & 0 \\ 0 & 0 & 0 & 0 \\ 0 & 0 & 0 & 1 \end{pmatrix}. \tag{6}$$

Its ground states are degenerate, and it spans a two-dimensional space with basis states $|00\rangle$ and $|10\rangle$. The adiabatically evolved ground state $|\psi_{f1}\rangle$ is the final state we are interested in. $|\psi_{f1}\rangle$ encodes the solution to the problem. The $|00\rangle$ and superposition states that contain a component in $|00\rangle$ can be ignored here because $|00\rangle$ has been removed from the initial state $|\psi_{b1}\rangle$. Thus, the solution to this two-qubit MSP is $|10\rangle$. Proving this solution is easy. The adiabatic total Hamiltonian is

$$H'_1(s) = (1 - s)H'_{b1} + sH_{f1}. \tag{7}$$

The four eigenvalues of $H'_1(s)$ are shown in Fig. 1. To simplify the NMR simulation of the adiabatic evolution, we modify the initial Hamiltonian in the following form:

$$H_{b1} = I - \begin{pmatrix} 0 & 0 & 0 & 0 \\ 0 & 1 & 0 & 1 \\ 0 & 0 & 1 & 1 \\ 0 & 1 & 1 & 0 \end{pmatrix}, \tag{8}$$

and the total Hamiltonian changes into

$$H_1(s) = (1 - s)H_{b1} + sH_{f1}. \tag{9}$$

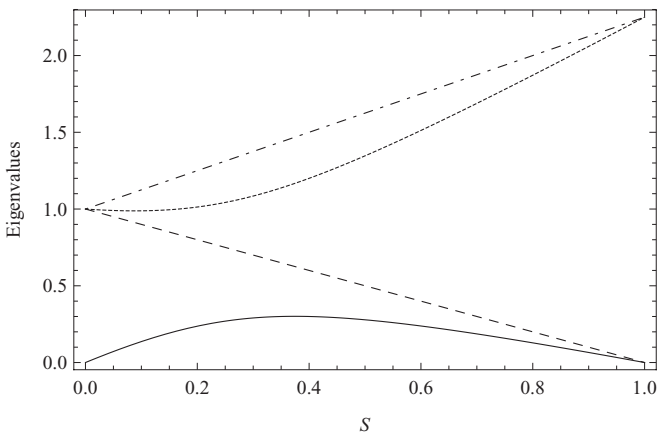

FIG. 1. Four eigenvalues of $H'_1(s) = (1 - s)H'_{b1} + sH_{f1}$.

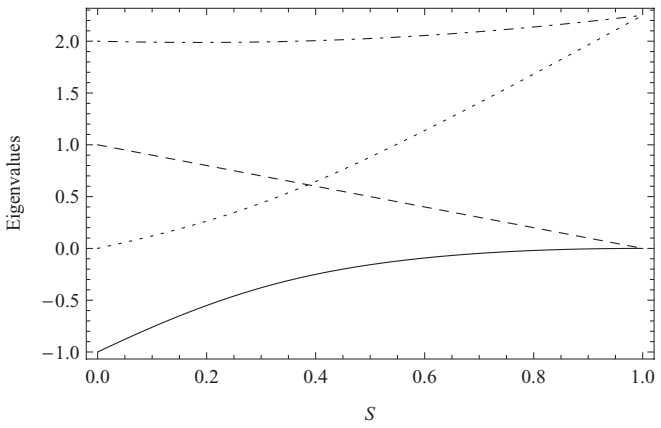

FIG. 2. Four eigenvalues of $H_1(s) = (1-s)H_{b1} + sH_{f1}$.

The ground state of H_{b1} can also easily be proven as $|\psi_{b1}\rangle$.

The four eigenvalues of $H_1(s)$, $\lambda_0(s)$ (solid line), $\lambda_1(s)$ (dotted line), $\lambda_2(s)$ (dashed line), and $\lambda_3(s)$ (dot-dashed line), which are labeled according to the increasing order from the lowest to the highest at $s = 0$, are shown in Fig. 2. Note that $\lambda_2(s)$ corresponds to the trivial solution 00. As $|00\rangle$ was removed from the initial state, the transition amplitude ε between $\lambda_0(s)$ and $\lambda_2(s)$ is zero. So, we should only consider the subspace expanded by $|01\rangle$, $|10\rangle$, and $|11\rangle$ and the crossing between $\lambda_1(s)$ and $\lambda_2(s)$ does not have any effect on the algorithm. In addition, the energy gap between the ground state $\lambda_0(s)$ and the excited state $\lambda_2(s)$ becomes zero as $s \to 1$. But no transition from $\lambda_0(s)$ to $\lambda_2(s)$ occurs, which is indicated by the fact that ε is zero. Thus, we only consider the gap between $\lambda_0(s)$ and $\lambda_1(s)$ for the calculation of the lower bound of T.

B. A symmetry-enhanced algorithm

A symmetry-enhanced algorithm can be constructed by using the method of enhanced symmetry of the Hamiltonian [43], and the method can be used to accelerate a large class of adiabatic quantum algorithms, which have exponential complexity [40–42]. These kinds of algorithms have a similar form, whose initial Hamiltonian is

$$H_b = I - |\alpha\rangle\langle\alpha|, \tag{10}$$

where

$$|\alpha\rangle = \frac{1}{\sqrt{2^n}} \sum_{i\in\{0,1\}^n} |i\rangle, \tag{11}$$

and the final Hamiltonian is

$$H_f = \sum_{i=1}^{N} f(i)|i\rangle\langle i|, \tag{12}$$

and $f:\{0,1\}^n \to R$ is a function which satisfies $|f(i)| \in O(\text{poly}(n))$, and the path of the varying Hamiltonian is

$$H(s) = (1-s)H_b + sH_f, \tag{13}$$

where $s = s(t)$ is a continuous function which satisfies $s(0) = 0$ and $s(T) = 1$.

According to (5) and (6), we should only consider H_{b1} and H_f in the subspace expanded by $|01\rangle$, $|10\rangle$, and $|11\rangle$. In this subspace, the ground state of H_{b1} is the equal superposition of all the basis states so does the ground state of (2), which is the initial state of Rao's algorithm.

The complexity of an adiabatic quantum algorithm is related to the structure of the Hamiltonian $H(s)$, especially the symmetry of it [43–45]. In Rao's algorithm, the structure of the initial Hamiltonian makes no reference to the final Hamiltonian [40]. The ground state of the initial Hamiltonian is the equal superposition of the computational basis states in the subspace, which does not have any structure characteristic with respect to the final Hamiltonian. Thus, there is no common symmetry in Eqs. (2) and (3), and the total Hamiltonian Eq. (4) does not have a structure symmetry.

If we enhance the symmetry of the total Hamiltonian, it may lead to a considerable acceleration of the adiabatic algorithm compared to quantum algorithms without symmetry [43]. Here, we propose an algorithm for MSP, which enhances the symmetry of the total Hamiltonian in Rao's algorithm. For this purpose, we set the initial Hamiltonian according to the final Hamiltonian which remains (3) in order to let them have the same symmetry. For example, in the two-bit case given in Table I, we modify the initial Hamiltonian to

$$H_{b2} = I - \frac{1}{2}\left(\sigma_x^1\sigma_x^2 + \sigma_y^1\sigma_y^2\right) = I - \begin{pmatrix} 0 & 0 & 0 & 0 \\ 0 & 0 & 1 & 0 \\ 0 & 1 & 0 & 0 \\ 0 & 0 & 0 & 0 \end{pmatrix}, \tag{14}$$

as the final Hamiltonian can be decomposed as

$$H_f = 9/4 \begin{pmatrix} 0 & 0 & 0 & 0 \\ 0 & 1 & 0 & 0 \\ 0 & 0 & 0 & 0 \\ 0 & 0 & 0 & 1 \end{pmatrix} = \frac{9}{8}\left(I - \sigma_z^2\right). \tag{15}$$

The total Hamiltonian is the linear interpolation,

$$H_2(s) = (1-s)H_{b2} + sH_f. \tag{16}$$

The new initial Hamiltonian and the final Hamiltonian have the same axial symmetry, which is invariant under a rotation around the z axis that transforms all σ_x^α's to $-\sigma_x^\alpha$'s where $\alpha = 1,2$. So, the total Hamiltonian $H_2(s)$ has the same symmetry as $[H_2(s), \sigma_z^1 + \sigma_z^2] = 0$. The ground state of the initial Hamiltonian is no longer the equal superposition of all the computational basis states, instead, it becomes $\frac{1}{\sqrt{2}}(|01\rangle + |10\rangle)$. The four eigenvalues of $H_2(s)$ are shown in Fig. 3.

The n-qubit final Hamiltonian of the adiabatic algorithm for the MSP, as given in Eq. (3), has only nonzero diagonal elements, and all nondiagonal elements are zero. It can be decomposed into a sum of the Pauli operators $\prod_{i=1}^n \sigma_{m_i}^i$, where $m_i = 3$ or 4 with $\sigma_3^i = \sigma_z^i$ and $\sigma_4^i = I$. Thus, we can set the n-qubit initial Hamiltonian to

$$-\sum_{i<j} f_{ij}\left(\sigma_x^i\sigma_x^j + \sigma_y^i\sigma_y^j\right), \tag{17}$$

the initial and final Hamiltonians have the same axial symmetry, which is invariant under rotations around the z axis.

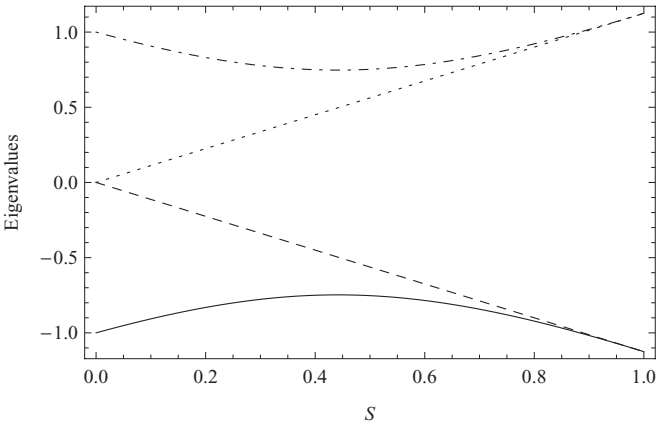

FIG. 3. Four eigenvalues of $H_2(s) = (1-s)H_{b2} + sH_{f2}$.

III. THE SIMULATION PROCEDURE

We implement the adiabatic quantum algorithms according to the method in Ref. [31] where the varying Hamiltonian is approximated via the quantum simulation technology [46], which recasts the adiabatic evolution using unitary operations. The continuously varying Hamiltonian $H(s)$ is discretized into $M+1$ steps, the value of s is equal to m/M at the mth step, and m goes from 0 to M. This unitary evolution can be written as

$$U = \prod_{m=0}^{M} U_m, \tag{18}$$

where U_m is the evolution operator of the mth step, which is given by

$$U_m = e^{-iH(s)\Delta t} = \exp\{-i[(1-m/M)H_b + (m/M)H_f]\Delta t\}, \tag{19}$$

where $\Delta t = T/(M+1)$. When both $T, M \to \infty$ and $\Delta t \to 0$, the adiabatic limit is achieved.

H_b and H_f do not generally commute. We can approximate U_m to the second order of Δt using the Trotter formula [46],

$$U_m \approx e^{-iH_f(m/M)\Delta t/2} e^{-iH_b(1-m/M)\Delta t} e^{-iH_f(m/M)\Delta t/2}. \tag{20}$$

Now, we study the simulation of Rao's algorithm for the two-qubit MSP. To perform the discrete unitary operation U_m in the NMR system, we decompose the initial Hamiltonian into spin operators [33],

$$H_{b1} = I - \tfrac{1}{2}\left[\left(I - \sigma_z^1\sigma_z^2\right) + \left(\sigma_x^1 - \sigma_x^1\sigma_z^2\right) + \left(\sigma_x^2 - \sigma_z^1\sigma_x^2\right)\right], \tag{21}$$

where the superscripts of σ_z and σ_x are used to label the qubits.

The final Hamiltonian,

$$H_f = \tfrac{9}{8}\left(I - \sigma_z^2\right) \tag{22}$$

is much simpler than the decomposition form of the initial Hamiltonian. Further decomposition of U_m into unitary operations can be implemented directly using NMR pulses. To obtain a neater expression, we let

$$\begin{aligned} &t_1 = (9m/4M)\Delta t, \quad t_2 = (1-m/M)\Delta t, \\ &I_x = \tfrac{1}{2}\sigma_x, \quad I_y = \tfrac{1}{2}\sigma_y, \quad I_z = \tfrac{1}{2}\sigma_z. \end{aligned} \tag{23}$$

Using the spin operator's transformation laws and the Trotter formula, we obtain

$$\begin{aligned} U_{m1} \approx\ & e^{iI_z^2(t_1/2)} e^{-iI_z^1 I_z^2 t_2} e^{iI_x^1(t_2/2)} (e^{-i(\pi/2)I_y^1} e^{-iI_z^1 I_z^2 t_2} e^{i(\pi/2)I_y^1}) \\ & \times e^{iI_x^2 t_2} (e^{-i(\pi/2)I_y^2} e^{-2iI_z^1 I_z^2 t_2} e^{i(\pi/2)I_y^2}) e^{iI_x^1(t_2/2)} \\ & \times (e^{-i(\pi/2)I_y^1} e^{-iI_z^1 I_z^2 t_2} e^{i(\pi/2)I_y^1}) e^{-iI_z^1 I_z^2 t_2} e^{iI_z^2(t_1/2)}, \end{aligned}$$

where the identity operator has been dropped because it does not produce any evolution of the quantum state and we only need consider the spin operator terms. Thus, we use 16 unitary operations in each step where the $e^{iI_\alpha t}$ term denotes a rotation along the α axis, where $\alpha = x, y, z$. The rotation along the z axis can be realized through the chemical shift evolution in the Hamiltonian of the system [47], and the rotations along the x and y axes are realized using hard pulses. The $e^{-iI_z^1 I_z^2 t_2}$ terms are realized using J-coupling evolution and refocusing pulses. All pulse sequences in the implementation of Rao's algorithm were optimized using a software compiler [47,48], which reduces the experimental errors.

We find the lower bound of T through numerical calculations. In detail, as shown in Fig. 2, the minimum energy gap between $\lambda_0(s)$ and $\lambda_1(s)$ is obtained, for $s \simeq 0.250$, to be $g_{\min} = 0.808$ and $\varepsilon = 1.237$. Therefore, $T \gg \frac{\varepsilon}{g_{\min}^2} = 1.897$, which is in the units of the natural time scale associated with the fundamental energy scale of the system [10,33].

The simulation of the SEA, which is with a higher symmetrical Hamiltonian, is the same as Rao's algorithm, except for the difference in U_m because of the change in the initial Hamiltonian. Through derivation, we obtain

$$\begin{aligned} U_{m2} \approx\ & e^{iI_z^2(t_1/2)} (e^{-i(\pi/2)I_y^1} e^{-i(\pi/2)I_y^2} e^{iI_z^1 I_z^2 t_2} e^{i(\pi/2)I_y^1} e^{i(\pi/2)I_y^2}) \\ & \times (e^{-iI_x^1(t_2/2)} e^{-i(\pi/2)I_x^2} e^{2iI_z^1 I_z^2 t_2} e^{i(\pi/2)I_x^1} e^{i(\pi/2)I_x^2}) \\ & \times (e^{-i(\pi/2)I_y^1} e^{-i(\pi/2)I_y^2} e^{iI_z^1 I_z^2 t_2} e^{i(\pi/2)I_y^1} e^{i(\pi/2)I_y^2}) e^{iI_z^2(t_1/2)}. \end{aligned}$$

The lower bound of the SEA is $T \gg 0.448$, where $g_{\min} = 1.494$ and $\varepsilon = 1.0$, which can be obtained through numerical calculations. In contrast, the lower bound of the run time of Rao's algorithm is 4.2 times the value of the SEA for the two-qubit MSP case. The symmetry-enhanced algorithm is more efficient than the algorithm without symmetry acceleration.

IV. EXPERIMENTAL IMPLEMENTATION

We demonstrated the adiabatic algorithms of the MSP in a two-qubit NMR system using a ^{13}C labeled $CHCl_3$ sample where the ^1H spin is assigned as the first qubit and the ^{13}C spin is the second. The experiments were implemented with a Bruker Avance III 400-MHz spectrometer at room temperature. The NMR system used here is a weakly coupled two-qubit system, and its Hamiltonian is

$$H = -\omega_1 I_{z1} - \omega_2 I_{z2} + 2\pi J_{12} I_{z1} I_{z2}, \tag{24}$$

where $\omega_1 = 3206.3$ and $\omega_2 = 7877.6$ Hz are the chemical shifts in ^1H and ^{13}C, respectively, and J_{12} is the indirect

coupling between the two spins, which has been measured as 215.2 Hz.

A. Experimental implementation of Rao's algorithm

The initial state was prepared from a pseudopure state $|00\rangle$ using a sequence of unitary operations where the pseudopure state was prepared from the thermal equilibrium state of the two-qubit system using the spatial averaging method [49–51]. The sequence is obtained via decomposing the unitary matrix that transforms $|00\rangle$ to $|\psi_{b1}\rangle$ as follows:

$$U = e^{i(\pi/4)I_y^2} e^{i(\pi/2)I_x^2} e^{-i(\pi/2)I_z^1 I_z^2} e^{-i(\pi/2)I_x^2} \times e^{-i2\cos^{-1}(1/\sqrt{3})I_y^1} e^{-i\pi I_x^2} e^{i(\pi/2)}. \quad (25)$$

The adiabatic evolution was simulated using $M+1$ steps of the unitary operations U_m. The adiabatic limit is achieved by letting both $T, M \to \infty$ and $\Delta t \to 0$. Steffen *et al.* [31] tested the behavior of the adiabatic algorithm by letting $T \to \infty$ and $M \to \infty$ while keeping Δt constant. Similarly, we explored the behavior of Rao's algorithm by letting $T, M \to \infty$ while keeping Δt at a small value. The number of Trotter steps were chosen from 15 to 55 every five steps. In the implementation of Rao's algorithm, Δt was chosen to be $T/(M+1) = 0.667$. Given Δt, T is obtained using $T = \Delta t \times (M+1)$, which is 5.27 times the lower bound at $M = 14$.

After the adiabatic evolution, the experimental density matrix of the final state was reconstructed via quantum state tomography [52–55]. Quantum state tomographic techniques have advanced considerably in recent years [56–58]. A two-qubit density matrix can be decomposed into the 16 two-qubit Pauli operators by $\rho = \Sigma_{L,R} LR\langle LR\rangle/4$, where $L, R \in \{I, \sigma_x, \sigma_y, \sigma_z\}$ and $\langle LR\rangle$ is the expectation value of LR. The tomographic outcome can be represented via the 16 real values $\langle LR\rangle$, which are the elements of the Pauli set [56] as shown in the following figures. The trivial $\langle II\rangle = 1$ is not shown in each figure.

The implementation fidelity P_{im}, simulated fidelity P_{sim}, and the total fidelity P_{tot} are defined as follows:

$$P_{\text{im}} = \text{Tr}(\rho_{\text{ex}}\rho_{\text{sim}}), \quad (26)$$

$$P_{\text{sim}} = \text{Tr}(\rho_{\text{sim}}\rho_{\text{th}}), \quad (27)$$

$$P_{\text{tot}} = \text{Tr}(\rho_{\text{ex}}\rho_{\text{th}}), \quad (28)$$

where ρ_{ex}, ρ_{sim}, and ρ_{th} are the density matrices of the final state obtained via experiment, numerical simulation, and theoretical prediction, respectively. ρ_{sim} was calculated using (20), whereas, ρ_{th} is $|10\rangle\langle 10|$, indicating the exact solution. And it can be proven that the value of each fidelity equals 1/4 times the dot product of the Pauli sets corresponding to the two density matrices in the trace [56].

The tomographic outcomes of the final state at $M = 14$ are shown in Fig. 4 with $P_{\text{sim}} = 96.14\%$, $P_{\text{im}} = 83.22\%$, and $P_{\text{tot}} = 81.76\%$. The Pauli set for $|10\rangle$ corresponding to the ideal solution with both $\langle ZI\rangle, \langle ZZ\rangle = -1$ and $\langle IZ\rangle = 1$ and the rest with $\langle LR\rangle = 0$, except for $\langle II\rangle$.

The final difference between the experimental outcome and the theoretical prediction consists of the errors of numerical approximation and that of the experimental implementation. These two parts of the errors come from different sources, the former results come from the theoretical approximation and the latter from control imperfection and decoherence. The error caused by the theoretical approximation consists of two parts. First, the evolution under the continuously varying Hamiltonian was approximated by discrete steps of unitary operations, whereas, the real adiabatic evolution corresponds to the adiabatic limit which demands both $T, M \to \infty$ and $\Delta t \to 0$, but in our theoretical approximation, T, M are finite, and $\Delta t > 0$. Second, the unitary operation of each Trotter step is approximated to the second order of the evolution time using the Trotter formula (20). The errors caused by the experimental implementation lead to the difference between the experimental outcome and the theoretical simulation, which is quantified via the experimental fidelity P_{im}.

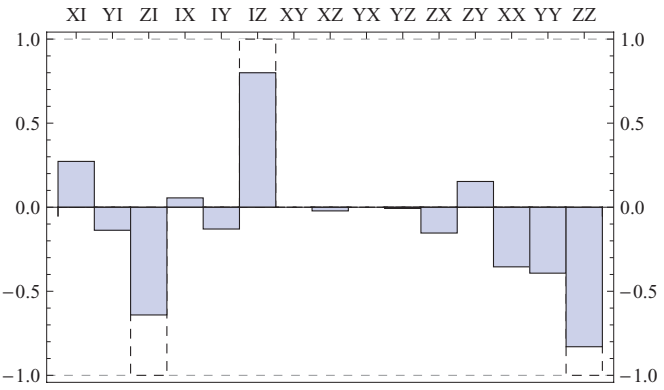

FIG. 4. (Color online) Experimental Pauli set for the final state of Rao's algorithm with $M = 14$, where X, Y and Z indicate σ_x, σ_y, and σ_z, respectively. The dashed bars correspond to the ideal state $|10\rangle$.

In the case of $M = 14$, $P_{\text{sim}} = 96.14\%$ reflects the error resulted from theoretical approximation with $T = 10$ and $\Delta t = 0.667$, whereas, $P_{\text{im}} = 83.22\%$ indicates the error induced by experimental implementation, and $P_{\text{tot}} = 81.76\%$ shows the deviation in the experimental outcome from the ideal solution.

We have estimated the errors by combining the experimental result and numerical simulation in the NMR spectrometer using one of the experiments. The error caused by the unwanted J coupling contributes 4.2%, the decoherence contributes 4.3%, and the control error contributes 8.3%. These numbers roughly give the influences of the different sources of errors in these experiments and are in line with other NMR experiments.

B. Analysis of the trade-off iteration number

With realizable control and real decoherence, the trade-off with increasing Trotter steps was studied. The experimental results are shown in Fig. 5, which plots the fidelity (triangles) as a function of M. We found that there is an optimal step number and run time of the algorithm from the plot at $M = 29$ and corresponding to 59 ms in time.

It is interesting to see the effect of gate imperfections and decoherence. The fidelity of the result obtained via numerical simulation using (20) increases with M when $M < 24$ as the simulation of evolution satisfying the adiabatic condition better when the number of iteration increases. Then, it reaches its maximum and stays around 99.60%. In experimental

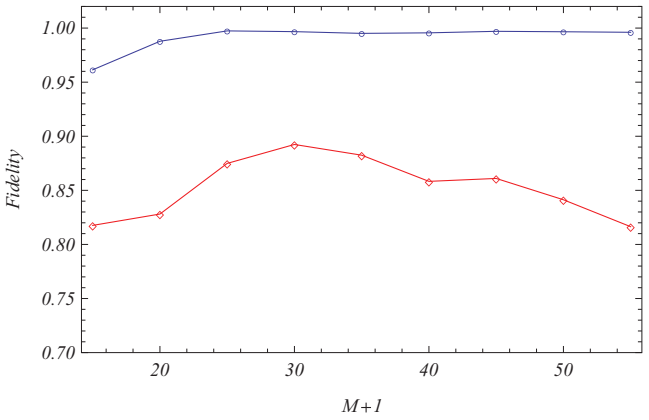

FIG. 5. (Color online) The relation between the fidelities and the number of Trotter steps. The circles represent P_{sim}, and the triangles represent P_{tot}.

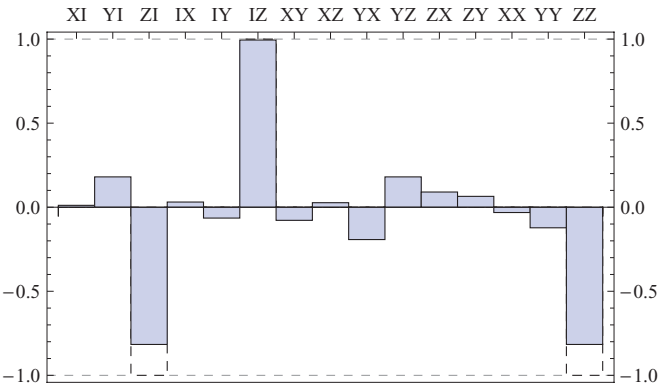

FIG. 6. (Color online) Experimental Pauli set for the final state of the SEA with $M = 14$ where X, Y, and Z indicate σ_x, σ_y, and σ_z, respectively. The dashed bars correspond to the ideal state $|10\rangle$.

implementation, due to the gate imperfections, the increase in the fidelity is delayed, and the maximum fidelity is achieved at $M = 29$. After that, the imperfection of pulses and decoherence may cause greater errors and spoils the benefits gained from the smoother adiabatic evolution. After $M > 29$, the imperfection of pulses and decoherence becomes dominant, so the performance of the adiabatic algorithm turns worse. There is a trade-off between satisfying the adiabatic condition versus the run time as shown in this experiment.

C. Experimental realization of the SEA

The initial state was prepared from the pseudopure state $|00\rangle$ using a sequence of unitary operations, which are $e^{-i\pi I_x^2}$, a Hadamard gate applied to the first qubit, and a controlled-NOT gate with the second qubit as the target qubit.

The SEA was implemented with $M = 14$. U_{m2} consists of 17 unitary operations at each Trotter step. T remained 10 as in Rao's algorithm. The experimental result is shown in Fig. 6. The fidelities of the experimental results at $M = 14$ for the two algorithms were compared. P_{tot} is 90.68% for the optimal algorithm, which is higher than 81.76% that gained via Rao's algorithm with the same T and M. And $P_{\text{sim}} = 99.02\%$, $P_{\text{im}} = 89.03\%$, which are all greater than that of Rao's algorithm at $M = 14$ and $T = 10$. P_{tot}, which is higher than P_{im} indicated that, in the experimental implementation, the output state is closer to the exact state, which has been found in another experiment [59] as expected when the gate operations refocus some of the inhomogeneities of the NMR system.

The better performance of the SEA than Rao's algorithm is due to the small lower bound on T in the SEA compared to that in Rao's algorithm. In the SEA, the lower bound is 0.448, whereas, in Rao's algorithm it is 1.897. Hence, with the same number of simulations and the same evolution time, the adiabatic condition is better satisfied in the SEA than in Rao's algorithm. Our experimental results have clearly demonstrated this.

V. CONCLUSIONS

To summarize, we have demonstrated two adiabatic quantum algorithms for the MSP in a two-qubit NMR system, which are Rao's algorithm and the SEA proposed in this paper. Both algorithms are successfully implemented, and both resolve the MSP. The experimental result of the SEA is better than Rao's algorithm with the same run time and number of Trotter steps. The agreement of the experimental results and their theoretical predictions confirms the applicability of the adiabatic quantum algorithms for the MSP. With realizable control and real decoherence, we studied the trade-off with increasing the Trotter steps in the experimental implementation of Rao's algorithm. We found that, as the number of steps increases, the adiabatic condition is satisfied better, however, the pulse imperfection and decoherence become worse and dominate the variation in the result fidelity from some step number. An optimal Trotter step number and run time were indicated by our results. The error of the experimental outcome results from environment decoherence and imperfect implementation.

ACKNOWLEDGMENTS

This work was supported by the National Natural Science Foundation of China (Grants No. 11175094 and No. 91221205) and the National Basic Research Program of China (Grants No. 2009CB929402 and No. 2011CB9216002). The authors also thank IQC, the University of Waterloo, for providing the NMR software compiler.

[1] P. Shor, in *Proceedings of the 35th Annual Symposium on Foundations of Computer Science* (IEEE, Los Alamitos, CA, 1994), p. 124.

[2] L. K. Grover, Phys. Rev. Lett. **79**, 325 (1997).

[3] D. Deutsch, Proc. R. Soc. London, Ser. A **425**, 73 (1989).

[4] R. Raussendorf and H. J. Briegel, Phys. Rev. Lett. **86**, 5188 (2001).
[5] E. Farhi, J. Goldstone, S. Gutmann, and M. Sipser, arXiv:quant-ph/0001106.
[6] E. Farhi, J. Goldstone, S. Gutmann, J. Lapan, A. Lundgren, and D. Preda, Science **292**, 472 (2001).
[7] G. L. Long, Commun. Theor. Phys. **45**, 825 (2006).
[8] A. M. Childs, E. Farhi, and J. Preskill, Phys. Rev. A **65**, 012322 (2001).
[9] J. Roland and N. J. Cerf, Phys. Rev. A **65**, 042308 (2002).
[10] S. Das, R. Kobes, and G. Kunstatter, Phys. Rev. A **65**, 062310 (2002).
[11] Z. Wei and M. Ying, Phys. Lett. A **354**, 271 (2006).
[12] M. V. P. Rao, Phys. Rev. A **67**, 052306 (2003).
[13] M. V. P. Rao, Phys. Rev. A **73**, 019902(E) (2006).
[14] E. Farhi, J. Goldstone, and S. Gutmann, arXiv:quant-ph/0208135.
[15] M. V. P. Rao, in *Proceedings of the 4th International Conference on Theory and Applications of Models of Computation*, Vol. 4484 (TAMC, Shanghai, China, 2007), p. 450.
[16] Z. Chen, P. W. Koh, and Y. Zhao, Phys. Rev. A **74**, 052314 (2006).
[17] W. van Dam, M. M. and U. Vazirani, in *Proceedings of the 42nd Annual Symposium on FOCS* (IEEE, Las Vegas, 2001), p. 279.
[18] D. Aharonov, W. v. Dam, J. Kempe, Z. Landau, S. Lloyd, and O. Regev, in *Proceedings of the 45th Annual IEEE Symposium on Foundations of Computer Science* (IEEE, Rome, 2004), p. 42.
[19] A. Mizel, D. A. Lidar, and M. Mitchell, Phys. Rev. Lett. **99**, 070502 (2007).
[20] S. P. Jordan, E. Farhi, and P. W. Shor, Phys. Rev. A **74**, 052322 (2006).
[21] D. A. Lidar, Phys. Rev. Lett. **100**, 160506 (2008).
[22] K. P. Marzlin and B. C. Sanders, Phys. Rev. Lett. **93**, 160408 (2004).
[23] D. M. Tong, K. Singh, L. C. Kwek, and C. H. Oh, Phys. Rev. Lett. **95**, 110407 (2005).
[24] D. M. Tong, K. Singh, L. C. Kwek, and C. H. Oh, Phys. Rev. Lett. **98**, 150402 (2007).
[25] D. M. Tong, Phys. Rev. Lett. **104**, 120401 (2010).
[26] Z. Wei and M. Ying, Phys. Rev. A **76**, 024304 (2007).
[27] Z. Wu and H. Yang, Phys. Rev. A **72**, 012114 (2005).
[28] S. Duki, H. Mathur, and O. Narayan, Phys. Rev. Lett. **97**, 128901 (2006).
[29] J. Ma, Y. Zhang, E. Wang, and B. Wu, Phys. Rev. Lett. **97**, 128902 (2006).
[30] K. P. Marzlin and B. C. Sanders, Phys. Rev. Lett. **97**, 128903 (2006).
[31] M. Steffen, W. van Dam, T. Hogg, G. Breyta, and I. Chuang, Phys. Rev. Lett. **90**, 067903 (2003).
[32] J. Du, L. Hu, Y. Wang, J. Wu, M. Zhao, and D. Suter, Phys. Rev. Lett. **101**, 060403 (2008).
[33] A. Mitra, A. Ghosh, R. Das, A. Patel, and A. Kumar, J. Mag. Res. **177**, 285 (2005).
[34] X. Peng, Z. Liao, N. Xu, G. Qin, X. Zhou, D. Suter, and J. Du, Phys. Rev. Lett. **101**, 220405 (2008).
[35] H. Chen, X. Kong, B. Chong, G. Qin, X. Zhou, X. Peng, and J. Du, Phys. Rev. A **83**, 032314 (2011).
[36] J. Du, N. Xu, X. Peng, P. Wang, S. Wu, and D. Lu, Phys. Rev. Lett. **104**, 030502 (2010).
[37] D. R. Simon, SIAM J. Comput. **26**, 1474 (1997).
[38] M. Ettinger and P. Hoyer, arXiv:quant-ph/9901029.
[39] O. Regev, SIAM J. Comput. **33**, 738 (2004).
[40] E. Farhi, J. Goldstone, S. Gutmann, and D. Nagaj, Int. J. Quantum Inf. **6**, 503 (2008).
[41] M. Znidaric and M. Horvat, Phys. Rev. A **73**, 022329 (2006).
[42] Z. Wei and M. Ying, arXiv:quant-ph/0604077.
[43] G. Schaller and R. Schtzhold, Quantum Inf. Comput. **10**, 109 (2010).
[44] J. I. Latorre and R. Orús, Phys. Rev. A **69**, 062302 (2004).
[45] R. Schützhold and G. Schaller, Phys. Rev. A **74**, 060304(R) (2006).
[46] H. F. Trotter, Pacific J. Math. **8**, 887 (1958).
[47] C. A. Ryan, C. Negrevergne, M. Laforest, E. Knill, and R. Laflamme, Phys. Rev. A **78**, 012328 (2008).
[48] A. M. Souza, J. Zhang, C. A. Ryan, and R. Laflamme, Nat. Commun. **2**, 169 (2011).
[49] D. G. Cory, A. F. Fahmy, and T. F. Havel, Proc. Natl. Acad. Sci. USA **94**, 1634 (1997).
[50] D. X. Wei, X. D. Yang, J. Luo, X. P. Sun, X. Z. Zeng, and M. L. Liu, Chin. Sci. Bull. **49**, 423 (2004).
[51] L. Hao, C. Wang, and G. L. Long, J. Phys. B **43**, 125502 (2010).
[52] M. G. Raymer, M. Beck, and D. F. McAlister, Phys. Rev. Lett. **72**, 1137 (1994); U. Leonhardt, *ibid.* **74**, 4101 (1995); D. Leibfried, D. M. Meekhof, B. E. King, C. Monroe, W. M. Itano, and D. J. Wineland, *ibid.* **77**, 4281 (1996).
[53] G. L. Long, H. Y. Yan, and Y. Sun, J. Opt. B: Quantum Semiclassical Opt. **3**, 376 (2001).
[54] J.-S. Lee, Phys. Lett. A **305**, 349 (2002).
[55] G. M. Leskowitz and L. J. Mueller, Phys. Rev. A **69**, 052302 (2004).
[56] J. M. Chow, L. DiCarlo, J. M. Gambetta, A. Nunnenkamp, L. S. Bishop, L. Frunzio, M. H. Devoret, S. M. Girvin, and R. J. Schoelkopf, Phys. Rev. A **81**, 062325 (2010).
[57] M. D. Shulman, O. E. Dial, S. P. Harvey, H. Bluhm, V. Umansky, and A. Yacoby, Science **336**, 202 (2012).
[58] J. A. Smolin, J. M. Gambetta, and G. Smith, Phys. Rev. Lett. **108**, 070502 (2012).
[59] J. Zhang, R. Laflamme, and D. Suter, Phys. Rev. Lett. **109**, 100503 (2012).